An Eigenvalue Perturbation Solution for the Multiphysics Simulation of Antenna Strain Sensors

Chunhee Cho, Xiaohua Yi, Dan Li, Yang Wang, *Member, IEEE*, and Manos M. Tentzeris, *Fellow, IEEE*

***Abstract*—To simulate the behavior of a passive antenna strain sensor, current multiphysics coupled simulation (between mechanics and electromagnetics) has mainly adopted the frequency domain solution. For every frequency point in the sweeping range, the frequency domain solver computes the value of scattering parameter S_{11}. The S_{11} curve is used to identify the new resonance frequency when the antenna sensor is at certain strain level. As a result, the frequency domain solution is computationally expensive. In this study, an eigenfrequency solution, whose efficiency is shown to be much higher than the frequency domain solver, is proposed to directly detect changes of antenna resonance frequency under strain. Toward the eigenfrequency solution, cavity and partially air-filled cavity FEM modeling techniques are proposed to reduce the number of degrees of freedom. In addition, by formulating the eigenfrequency solution as an eigenvalue perturbation problem, Rayleigh quotient iteration and the inverse power iteration method with Rayleigh quotient are proposed to further improve the computational efficiency. The proposed methods will greatly improve the efficiency of antenna sensor designs.**

***Index Terms*—Air-filled cavity, antenna sensor, eigenvalue perturbation, inverse power iteration method (IPIRQ), multiphysics simulation, Rayleigh quotient iteration (RQI).**

I. Introduction

AMONG the great variety of structural health monitoring technologies, passive wireless sensing has obvious advantages. A passive (battery-free) wireless sensor requires neither cable nor external power supply for operation [1]–[5]. There are two categories of passive wireless sensing technologies for strain and crack sensing. The first one utilizes resonating circuits consisting of inductors, capacitors, and resistors [6]–[8]. In this category, the sensor interrogation is achieved by inductive coupling, a near field effect. Therefore, the wireless interrogation distance is usually limited to a few inches, which is inconvenient for practical applications. The second category relies on far-field effect to characterize changes in antenna properties, including resonance frequency, power spectrum, and return loss [9]–[11]. When an antenna experiences strain deformation, the antenna shape changes causing shift in electromagnetic resonance frequency of the antenna. For example, authors have developed passive radio frequency identification (RFID) antenna sensors for wireless strain measurement [12], [13]. Through signal modulation by an economic RFID chip (costing about $0.10), the RFID antenna sensors achieve much longer interrogation distances than inductive coupling sensors, and demonstrate promising performance for wireless strain/crack sensing. In another example, a frequency doubling technique is introduced as an alternative approach for signal modulation of a passive antenna sensor [14], [15].

In order to accurately describe the electromagnetic behaviors of these antenna sensors under strain, it is essential to consider two physical domains: electromagnetics (antenna resonance frequency) and mechanics (strain) [16]. In the multiphysics simulation, the mechanical simulation is conducted for a certain strain level first. The deformed shape of the antenna structure is directly used for electromagnetic simulation through moving meshes, which transfer the actual deformed shape to the electromagnetic simulation. The resonance frequency of an antenna is determined by sweeping through a large frequency range and identifying the minimum point from the scattering parameter (S_{11}) plot. During the final stage of a sensor design, the frequency-domain simulation is necessary for verifying antenna radiation performance. Although frequency-domain simulation is a common practice, it is time consuming and inefficient, particularly when the performance of an antenna sensor needs to be characterized at many strain levels. In this paper, an eigenfrequency solution is proposed to directly detect resonance frequency change of an antenna sensor under strain, without the time consuming computation of S_{11} plot at many different strain levels. The eigenfrequency solution significantly reduces simulation time while maintaining the simulation accuracy for strain sensing. In addition, two novel approaches are proposed to further improve simulation speed in this paper, one through the simulation model and the other through eigenfrequency solver.

In FE modeling of electromagnetics, a full-wave model is generally used because it can describe not only resonance frequencies but also other antenna parameters. These include antenna gain, as well as electric and magnetic radiations in near and far fields. However, the full-wave model is computationally expensive because oftentimes hundreds of thousands of degrees of freedom (DOFs) are needed for accuracy [12], [15], [16]. In this paper, the cavity and partially air-filled cavity models are proposed to reduce the number of DOFs from a full-wave model

Manuscript received September 26, 2016; revised January 10, 2017 and March 9, 2017; accepted April 12, 2017. Date of publication April 26, 2017; date of current version May 12, 2017. This work was supported by the Air Force Office of Scientific Research under Grant FA9550-14-1-0054. *(Chunhee Cho and Xiaohua Yi are co-first authors.) (Corresponding author: Chunhee Cho.)*

C. Cho, D. Li, Y. Wang, and M. M. Tentzeris are with the School of Civil and Environmental Engineering, Georgia Institute of Technology, Atlanta, GA 30332 USA (e-mail: ccho37@gatech.edu; dli323@gatech.edu; yang.wang@ce.gatech.edu; etentze@ece.gatech.edu).

X. Yi was with the School of Civil and Environmental Engineering, Georgia Institute of Technology, Atlanta, GA 30332 USA. He is now with the ExxonMobil Upstream Research Company, Houston, TX 77389 USA (e-mail: yixhzju@gmail.com).

Digital Object Identifier 10.1109/JMMCT.2017.2698338

2379-8793 © 2017 IEEE. Personal use is permitted, but republication/redistribution requires IEEE permission.
See http://www.ieee.org/publications_standards/publications/rights/index.html for more information.

[17], [18]. The cavity model reduces computational loads by simply removing the air volume, and thus, all air elements. For the partially air-filled cavity model, although an air domain still exists, the size of the air box is much smaller than the air volume of the full-wave model. In the boundary conditions to truncate the simulation domain, while the full-wave model commonly uses perfectly matched layers (PMLs) to require several mesh layers, both new models use perfect electric conductor (PEC) and perfect magnetic conductor (PMC) to be defined by only one layer. As a result, the proposed eigenfrequency solution with cavity or partially air-filled cavity model requires order-of-magnitude less computing time compared with the common approach of simulating S_{11} plots of a full-wave model at multiple strain levels. This paper will also examine the accuracy of the proposed models and eigenfrequency solution.

In order to further improve computing speed in antenna sensor design, this paper also investigates a number of eigenvalue perturbation algorithms for finding eigenfrequency at a new strain level. As the antenna sensor deforms under strain, the finite element model computes deformed geometries to generate the new inductance and capacitance matrices of the antenna. The eigenfrequency algorithms utilize results from a previous step as a starting point, viewing the eigenvalue problem at the next strain level as a small perturbation to the previous strain level. Based on the commonly used Rayleigh quotient iteration (RQI) method, we propose an inverse power iteration method with Rayleigh quotient (IPIRQ) [19]–[21]. Rapid solution of the eigenvalue problem provides the shifted resonance frequency of the antenna sensor at the new strain level. These proposed eigenvalue perturbation algorithms allow the resonance frequencies of the antenna sensor to be rapidly identified at many strain levels. As a result, the strain sensitivity of the antenna sensor can be immediately calculated as the slope of the (approximately) linear relationship between resonance frequency and strain level.

The rest of this paper is organized as follows. Section II describes finite element formulation of the eigenfrequency (eigenvalue) problem for antenna sensors. Section III compares the computing load and accuracy of three FEM electromagnetic models, including full-wave, cavity, and partially air-filled cavity models. Section IV presents RQI and IPIRQ techniques. Section V shows a validation example of the proposed methods with a 2.9 GHz patch antenna. Finally, the paper is summarized with a conclusion and future work.

II. Finite Element Formulation of the Eigenvalue Problem

This section describes the finite element formulation and its eigenfrequency solution of antenna sensors. Section II-A introduces the basic finite element formulation in electromagnetic problems. Section II-B presents the eigenfrequency solution from state-space formulation. Section II-C compares the simulation efficiency of the eigenfrequency solution and the frequency domain solution.

A. Finite Element Formulation

For simulating an antenna strain/crack sensor, Fig. 1 illustrates the domains including the sensor, an air sphere, and PML.

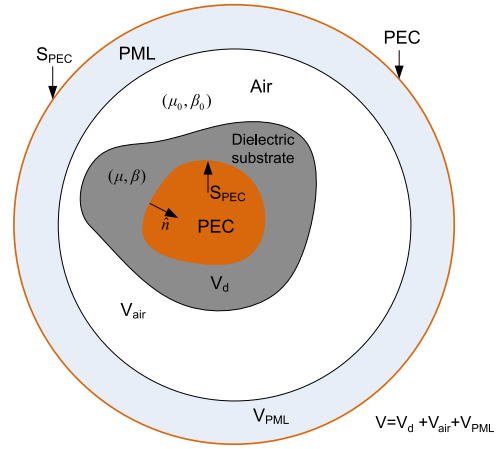

Fig. 1. Inhomogeneous structure enclosed by termination boundaries.

A patch antenna sensor usually includes a top metallic surface, a dielectric substrate layer in the middle, and a bottom ground plane for attaching to the structure being monitored. The substrate material affects antenna radiation performance and antenna size. The metallic surface is usually modeled as PEC materials. The boundary of the metallic surface is denoted as S_{PEC}, whose direction is $\hat{n}$. The volume of the dielectric substrate is denoted as V_d and the substrate relative permeability and permittivity are μ_r and β_r, respectively. The entire antenna sensor is placed inside an air sphere, whose permittivity and permeability are μ_0 and β_0, respectively. Since a resonant antenna model is an open structure that has no definite physical boundaries, it is necessary to set termination boundaries so that the simulation domain is finite. The combination of PML and PEC is adopted in the 3-D electromagnetic simulation. The Maxwell's equations in an inhomogeneous material have the general vector form [22], [23]

$$\begin{aligned} \nabla \times E &= -j\omega\mu H \\ \nabla \times H &= j\omega\beta E + J \\ \nabla \cdot (\beta E) &= \rho \\ \nabla \cdot (\mu H) &= 0 \end{aligned} \tag{1}$$

where $\mathbf{E} = E_x\,\hat{\mathrm{x}} + E_y\hat{\mathrm{y}} + E_z\hat{\mathrm{z}}$ is the electric field; $\mathbf{H} = H_x\,\hat{\mathrm{x}} + H_y\hat{\mathrm{y}} + H_z\hat{z}$ is the magnetic field; $\mathbf{J}$ is the current vector; ρ is charge density; μ and β are the permeability and permittivity of the material, respectively; ω is the angular frequency; ∇ is the del operator in Cartesian coordinates

$$\nabla = \hat{\mathrm{x}}\frac{\partial}{\partial \mathrm{x}} + \hat{\mathrm{y}}\frac{\partial}{\partial \mathrm{y}} + \hat{\mathrm{z}}\frac{\partial}{\partial \mathrm{z}}. \tag{2}$$

In finite element method, the entire solution domain is discretized into a finite number of elements. Each element occupies a separate volume V^e ($e = 1, 2, \ldots, N_{\mathrm{T}}$), where N_{T} is the total number of elements. The electric field can then be denoted in a vector form in terms of the polynomial basis functions $\boldsymbol{N}_i^e$ over a general m-edge finite element [22]

$$E^e = \sum_{i=1}^{m} E_i^e N_i^e \tag{3}$$

where $\mathbf{N}_i^e$ is the *i*th edge based vector basis function of element *e*; *m* is the total edge number of one element; E_i^e is the tangential electric field along the *i*th edge of element *e*. According to variational principle, the following discretized equation can be obtained [24]:

$$(j\omega)^2 \sum_{e=1}^{N_T} [T^e]\{E^e\} + (j\omega) \sum_{e=1}^{N_T} [R^e]\{E^e\} + \sum_{e=1}^{N_T} [C^e]\{E^e\} = \sum_{e=1}^{N_T} \{p^e\} \tag{4}$$

where μ is the permeability; ω is angular frequency; $[C^e]$, $[R^e]$, and $[T^e]$ are elementary inductance, damping, and capacitance matrix, respectively; p^e is the source term due to incident voltage or current excitation at the port. The entries of the matrix, $[C^e]$, $[R^e]$, and $[T^e]$ are given by

$$C_{ij}^e = \int_{V^e} \frac{1}{\mu} (\nabla \times N_i^e) \cdot (\nabla \times N_j^e)\, dv$$
$$R_{ij}^e = \mu \left[\int_{S^e} N_i^e \cdot (\hat{n} \times N_j^e)\, dS \right]$$
$$T_{ij}^e = \int_{V^e} \beta N_i^e \cdot N_j^e dv \tag{5}$$

where V^e is the volume of element *e*; S^e is the boundary of element *e*.

B. Eigenfrequency Solution

If no excitation is considered, the source term $\{p^e\}$ in (4) vanishes. The equation can be rewritten as [22] with simplification as follows

$$\lambda^2 [\mathrm{T}]\{\mathrm{E}\} + \lambda [\mathrm{R}]\{\mathrm{E}\} + [\mathrm{C}]\ \{\mathrm{E}\} = \{0\} \tag{6}$$

where λ is eigenvalue; [C] is named as inductance matrix; [T] is named as capacitance matrix, while [R] is the damping matrix. The final formulation in (6) ends up as a quadratic eigenvalue problem [25], [27]. Using *N* to denote the total number of DoFs in (6), [C] and [R] are N × N complex symmetric matrices, while [T] is an N × N real symmetric matrix. Since the entry T_{ij}^e in (5) includes material permittivity β, which is a small number on the order of 10^{-12}, the magnitudes of T_{ij}^e as well as entries in global matrix [T] are small. The entry R_{ij}^e in (5) is also small due to small magnitude of μ_0. With small-magnitude entries in [R] and [T], the matrices are usually ill-conditioned. To improve the condition number of the two matrices, a scaling factor is empirically determined as follows:

$$s = 1{,}000 \times \frac{\max_{i,j} |\mathrm{C}_{i,j}|}{\max_{i,j} |\mathrm{T}_{i,j}|}. \tag{7}$$

To this end, (6) is reformulated as

$$\tilde{\lambda}^2 [\mathrm{T^s}]\{\mathrm{E}\} + \tilde{\lambda} [\mathrm{R^s}]\{\mathrm{E}\} + [\mathrm{C}]\ \{\mathrm{E}\} = \{0\} \tag{8}$$

where

$$[R^s] = \sqrt{s}\,[R] \qquad [T^s] = s\,[T] \qquad \tilde{\lambda} = \lambda/\sqrt{s}. \tag{9}$$

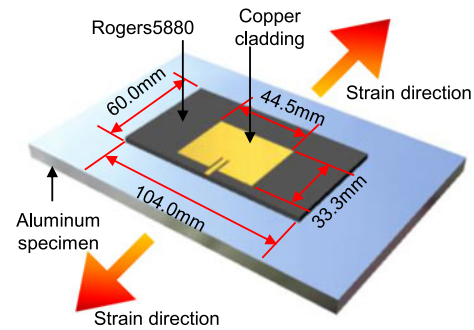

Fig. 2. Illustration of the 2.9 GHz patch antenna on the aluminum specimen.

State-space formulation equivalently converts (6) into a generalized eigenvalue problem

$$[\mathrm{A}]\ \{\Phi\} = \tilde{\lambda}\ [\mathrm{B}]\{\Phi\} \tag{10}$$

where

$$[\mathrm{A}] = \begin{bmatrix} -[\mathrm{C}] & [0] \\ [0] & [\mathrm{T^s}] \end{bmatrix} \qquad [\mathrm{B}] = \begin{bmatrix} [\mathrm{R^s}] & [\mathrm{T^s}] \\ [\mathrm{T^s}] & [0] \end{bmatrix} \qquad \{\Phi\} = \begin{Bmatrix} \{\mathrm{E}\} \\ \tilde{\lambda}\{\mathrm{E}\} \end{Bmatrix} \tag{11}$$

Here [0] is an N×N zero matrix.

The eigenvalue λ is closely related with resonance frequency of the antenna sensor f_{R} according to the following equation:

$$\tilde{\lambda} = \frac{\mathrm{j}\omega - a}{\sqrt{s}} = \frac{\mathrm{j}2\pi f_R - a}{\sqrt{s}}. \tag{12}$$

The resonance frequency f_{R} is a key parameter determining the strain effects of the antenna sensor. Real value a is used to determine the quality factor for antenna design. Associated with every eigenvalue λ, eigenvector $\{\Phi\}$ represents the electric field distribution of each eigenmode.

C. Comparison of Eigenfrequency and Frequency Domain Solutions

In order to compare performances of two solutions for strain sensing simulation, i.e., the eigenfrequency solution and the frequency domain solution, a 2.9 GHz patch antenna is modeled as an example using the commercial multiphysics software package COMSOL (see Fig. 2). The substrate material of the example model is Rogers RT/duriod 5880 with dielectric constant ($\varepsilon_r = 2.2$) and low loss tangent of 0.0009. The thickness of the substrate is 0.7874 mm and the planar dimension of the 2.9 GHz patch antenna is 44.5 mm × 33.3 mm. The antenna is mounted on an aluminum specimen. Strain is applied to the two ends of the aluminum specimen. The 3-D full-wave electromagnetic simulation setup of the 2.9 GHz model for COMSOL is presented in Fig. 3(a). PEC boundaries are assigned to the outside of the air sphere, the patch, and the ground plane. The PML boundary is also combined with the PEC at the air sphere. The total number of DOFs is 259 975. Simulations are conducted on a desktop with Intel Xeon processor E5-1620V3 (four cores, 3.5 GHz) and 16 GB RAM memory.

At first, the frequency domain solver simulates a scattering parameter S_{11} plot [see Fig. 3(b)]. This is an indicator of the antenna radiation performance in the sweeping frequency ranges at different strain levels from zero to 2000 $\mu\varepsilon$, with 500 $\mu\varepsilon$

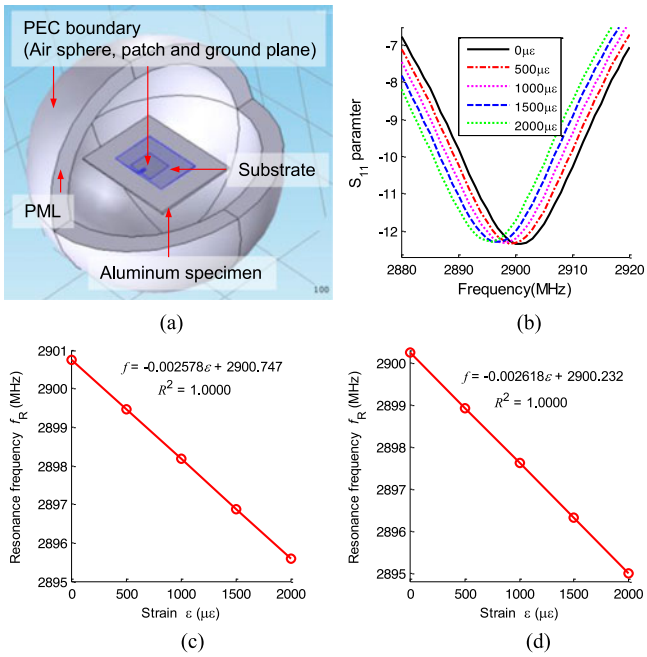

Fig. 3. Comparison between frequency domain and eigenfrequency solvers in the full-wave model. (a) Full-wave model. (b) S_{11} parameter (frequency domain solver). (c) Resonance frequency versus strain (frequency domain solver). (d) Resonance frequency versus strain (eigenfrequency solver).

strain increase per step. The computation of S_{11} curve at each strain level is performed for 51 frequency points, consuming 9722 s (2 h, 42 min, 2 s) in total. The minimum valley point of a S_{11} plot presents the resonance frequency of the antenna at that strain level. As a postprocessing procedure, linear regression is performed between resonance frequency and strain to construct the strain sensitivity plot [see Fig. 3(c)]. The resonance frequency is 2900.75 MHz and strain sensitivity is -2578 Hz/$\mu\varepsilon$, which means 1 $\mu\varepsilon$ strain experienced by the patch antenna introduces a frequency change of -2578 Hz. The coefficient of determination is close to 1.0000, which shows a highly linear relationship.

In the eigenfrequency solution, COMSOL LiveLink interface for MATLAB is adopted [28]. The mechanics simulation for certain strain level is conducted first in the mechanical domain. Through the LiveLink, the $[C]$, $[R]$, and $[T]$ from COMSOL are transferred into the MATLAB, which formulates $[A]$ and $[B]$ matrix [see (10) and (11)]. Finally MATLAB `eigs` command is used to compute the generalized eigenvalue solution of these sparse $[A]$ and $[B]$ matrix [28]. The `eigs` command is set to directly search the eigenfrequency close to 2900 MHz. The eigenfrequency is again extracted for each strain level. After performing linear regression between resonance frequency and strain data, the strain sensitivity is identified as $-2{,}618$ Hz/$\mu\varepsilon$ and resonance frequency at zero strain level is 2900.23 MHz [see Fig. 3(d)]. These are very close to the frequency-domain results. The coefficient of determination is also rounded off to 1.0000. The computing time at each strain level is 520 s (8 min 40 s) for the eigenfrequency solver, which is much faster than the frequency-domain solver. Therefore, it is demonstrated

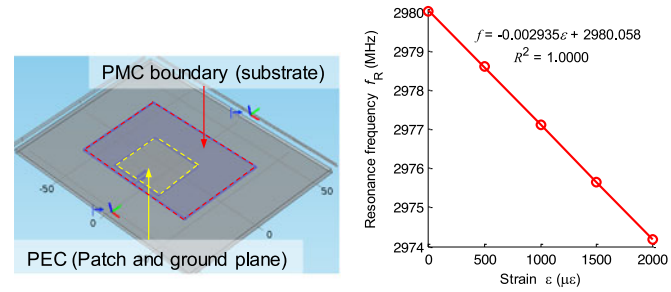

Fig. 4. Cavity model simulation. (a) Cavity model. (b) Resonance frequency versus strain.

that the strain sensitivity simulation, the efficiency of the eigenfrequency solver is nearly 20 times higher than the frequency-domain solver.

III. FEM Modeling Techniques to Improve Simulation Efficiency

This section describes two electromagnetic FEM modeling techniques to reduce computational efforts with much less number of DOFs. Section III-A presents a cavity model, which removes the air volume from the full-wave model to reduce DOFs. However, it was observed that the cavity model cannot consider fringing effect due to the lack air volume. In order to address this problem, Section III-B describes a partially air-filled cavity model which has a shallow air box on the patch antenna to compensate the fringing effect, without significantly increasing the number of DOFs.

A. Cavity Model

Although the eigenfrequency solution in the full-wave model provides similar results as the frequency-domain results, many spurious modes exist along with the resonance mode. Therefore, it can be difficult to identify the correct resonance mode and the corresponding frequency. By removing the air sphere and modifying boundary conditions correspondingly, a cavity model entails much less DOFs than the full-wave model. The cavity model of the 2.9 GHz patch antenna is shown in Fig. 4(a). PEC boundaries are assigned as the microstrip patch and a ground plane. PMC boundaries are assigned to four sides and the top of the substrate. These boundary conditions exclude the aluminum plate in this electromagnetic domain simulation although the plate still exists in the mechanical simulation. Therefore, while electromagnetic domain of the full-wave model contains the aluminum plate and the air, the cavity model contains only the patch antenna and achieves faster computing. The total number of DOFs is 24 459, which is about ten times smaller than that of the full-wave model.

Benefiting from much less DOFs, total computing time of the eigenfrequency solver at each strain level is only 8 s. However, because PMC boundary conditions are assigned on the substrate, a fringing field is not generated around the side of the microstrip patch in the cavity model. Therefore, the simulated resonance frequency at zero strain is 2980.06 MHz [see Fig. 4(b)], which is

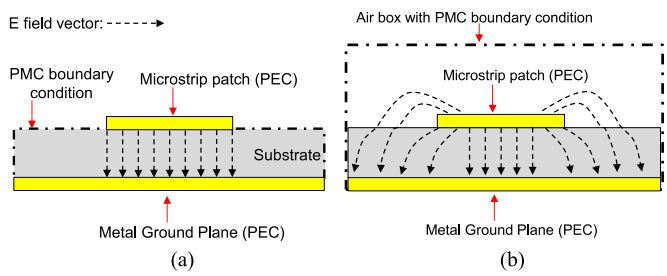

Fig. 5. Electric field comparison. (a) Cavity model. (b) Partially air-filled cavity model.

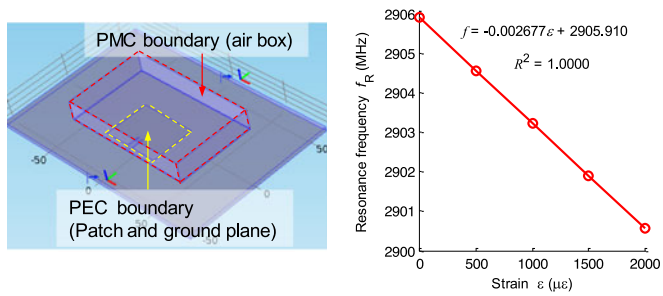

Fig. 6. Partially air-filled cavity model simulation. (a) Partially air-filled cavity model. (b) Resonance frequency versus strain.

2.7% different from resonance frequency of the full-wave model in Section II. Fig. 4(b) shows the simulated strain sensitivity to be -2,935 Hz/$\mu\varepsilon$, which is also 12.1% higher than the full-wave model. In conclusion, although the cavity model requires less computation, this approach has notable inaccuracy because of neglecting the fringing effect.

B. Partially Air-Filled Cavity Model

By adding a small air box to the cavity model, the fringing field is restored in the electromagnetics simulation. Fig. 5 explains the electric field comparison between a cavity and a partially air-filled cavity model. The cavity model assigns PMC boundaries on the surface of the substrate, which blocks the generation of the electric field in the horizontal direction. In other words, the direction of the electrical field is only vertical [see Fig. 5(a)]. The partially air-filled cavity model assigns PMC boundary conditions on the added air box, which provides enough space for generating the horizontal electrical field [see Fig. 5(b)]. Therefore, the partially air-filled cavity model is able to describe the fringing field.

The partially air-filled cavity model of the 2.9 GHz patch antenna is simulated in COMSOL (see Fig. 6). PEC boundary conditions are the same as in the cavity model in Section III-A, and PMCs are assigned on the surface of the air box [see Fig. 6(a)]. The number of DOFs is 56,379. Although this number is larger than that of the cavity model, it is still five times smaller than the full-wave model. As shown in Fig. 6(b), simulated resonance frequency is 2905.91 MHz, which is much closer to the resonance frequency from the full-wave model. Strain sensitivity is calculated as $-2{,}677$ Hz/$\mu\varepsilon$ and the coefficient of determination is close to 1.0000. The computing time at each strain level of the eigenfrequency solver is 25 s. The comparison among three FEM models in Sections II and III is briefly summarized in Table I. The partially air-filled cavity model is shown to achieve the best tradeoff between computing time and accuracy.

TABLE I
COMPARISON OF THREE FEM MODELS

	Full-wave model	Cavity model	Partially air- filled cavity model
Resonance frequency	2900.23 MHz	2980.06 MHz (∗error: 2.75%)	2905.91 MHz (∗error: 0.20%)
Strain sensitivity	-2618 Hz/$\mu\varepsilon$	-2935 Hz/$\mu\varepsilon$ (∗error:12.12%)	-2677 Hz/$\mu\varepsilon$ (∗error: 2.25%)
No. of DOFs	259 975	24 459	56 379
Eigenfrequency solution time at each strain level	520 s	8 s	25 s

∗ Errors are relative to the full-wave model

IV. EIGENFREQUENCY SOLVERS FOR STRAIN SENSING SIMULATION

In the strain sensing simulation, because changes of system matrices [A] and [B] between two adjacent strain levels are expected to be small, the differences in eigenfrequencies and eigenvectors are likewise small. In order to reach fast convergence, the eigenvalues and eigenvectors in the previous step can be utilized as starting vectors to search for solution at the next strain step. Section IV-A explains the RQI method, a commonly used eigenvalue algorithm. In Section IV-B, we proposed an IPIRQ method, which can be implemented to further improve the solution speed. Section IV-C describes the overall COMSOL-MATLAB framework for strain sensing simulation using these eigenvalue perturbation algorithms.

A. RQI Method

The RQI method is implemented to improve computational efficiency of the eigenfrequency solution. To find the interested eigenfrequency of an antenna resonance mode, the shifted version of RQI is implemented (see Fig. 7).

As described in (11), [A] and [B] are complex-valued symmetric and sparse matrices. Since matrix with a smaller bandwidth generally improves speed of linear solvers, the reverse Cuthill-McKee algorithm [29] is applied to [A] and [B] first in step ①, producing a preordering permutation matrix [P] and preordered matrices $[\tilde{A}_{j+1}]$ and $[\tilde{B}_{j+1}]$ with smaller bandwidth. In step ②, since the generalized eigenvalue is not affected by the preordering process, λ_j at strain level ε_j is directly saved as an intermediate eigenvalue μ for starting the search. Meanwhile, the starting eigenvector $\{q\}$ is determined by reordering eigenvector $\{\Phi_j\}$ with permutation matrix [P]. In step ③, a temporary scaler d is computed once for later repetitive use in the `do-while` loop. In step ④, the LU factorization is performed with $[\tilde{A}_{j+1}] - \mu[\tilde{B}_{j+1}]$ to obtain a lower triangular

① Preordering $[\mathrm{P}][\mathrm{A}_{j+1}][\mathrm{P}]^{\mathrm{T}} = [\tilde{\mathrm{A}}_{j+1}]$;
$[\mathrm{P}][\mathrm{B}_{j+1}][\mathrm{P}]^{\mathrm{T}} = [\tilde{\mathrm{B}}_{j+1}]$;

② $\mu = \lambda_j$; $\{q\} = [\mathrm{P}]\{\Phi_j\}$;

③ $d = \|[\tilde{\mathrm{A}}_{j+1}]\| + \|\mu[\tilde{\mathrm{B}}_{j+1}]\|$;

do {

④ LU factorization $([\tilde{\mathrm{A}}_{j+1}] - \mu[\tilde{\mathrm{B}}_{j+1}]) = [\mathrm{L}][\mathrm{U}]$;

⑤ $\{q\} = [\mathrm{U}^{-1}][\mathrm{L}^{-1}][\tilde{\mathrm{B}}_{j+1}]\{q\}$;

$\{q\} = \dfrac{\{q\}}{\|\{q\}\|}$;

⑥ $\mu = \dfrac{\{q\}^{\mathrm{H}}[\tilde{\mathrm{A}}_{j+1}]\{q\}}{\{q\}^{\mathrm{H}}[\tilde{\mathrm{B}}_{j+1}]\{q\}}$;

⑦ error $= \dfrac{\|[\tilde{\mathrm{A}}_{j+1}]\{q\} - \mu[\tilde{\mathrm{B}}_{j+1}]\{q\}\|}{d}$;

} **while** (error > tolerance);

⑧ $\lambda_{j+1} = \mu$; $\{\Phi_{j+1}\} = [\mathrm{P}]^{\mathrm{T}}\{q\}$;

Fig. 7. RQI routine for shifted symmetric [A] and [B] formulations.

matrix [L] and upper triangular matrix [U]. This LU factorization is the most computationally expensive step in RQI process. In step ⑤, the intermediate eigenvector $\{q\}$ is updated and normalized. In step ⑥, the intermediate eigenvalue μ is updated by the Rayleigh quotient. In step ⑦, the error of the current step is calculated. If the error is lower than tolerance, the loop terminates; the eigenvalue λ_{j+1} and eigenvector $\{\Phi_{j+1}\}$ at strain level ε_{j+1} are updated in step ⑧. To restore the original eigenvector order, the intermediate eigenvector $\{q\}$ is reordered by the transpose of the permutation matrix $[\mathrm{P}]^{\mathrm{T}}$. If the error is higher than tolerance, the algorithm returns to step ④ and iterates the process.

B. IPIRQ Method

Although the RQI method is commonly used, an IPIRQ method is proposed to herein further improve computing speed. In the RQI method, the most computationally expensive step is the LU factorization. When the RQI method iterates in the `do-while` loop, the LU factorization is computed in every iteration, increasing computational loads. In comparison, the proposed IPIRQ method performs the factorization only one time and effectively reuses factorization results ([L] and [U] matrices) for each iteration. Therefore, the IPIRQ method can be much faster than the RQI method in most cases [21].

The process of the IPIRQ from step ① to ③ is the same as the RQI method in Fig. 7. But, in step ④, the LU factorization is moved out of the `do while` loop, and placed before `do`. The process from step ⑤ to ⑧ also follows the RQI method. Compared with the RQI method, the [L] and [U] matrices used at step ⑤ of the IPIRQ method are only accurate at first iteration. At the second or any later iteration, the RQI performs factorization to $[\tilde{\mathrm{A}}_{j+1}] - \mu[\tilde{\mathrm{B}}_{j+1}]$ with the updated μ value, to get updated [L] and [U]. However, IPIRQ reuses the [L] and [U] from the first iteration as approximation to these two matrices at the current iteration. Therefore, despite time saving, the accuracy of IPIRQ is yet to be examined.

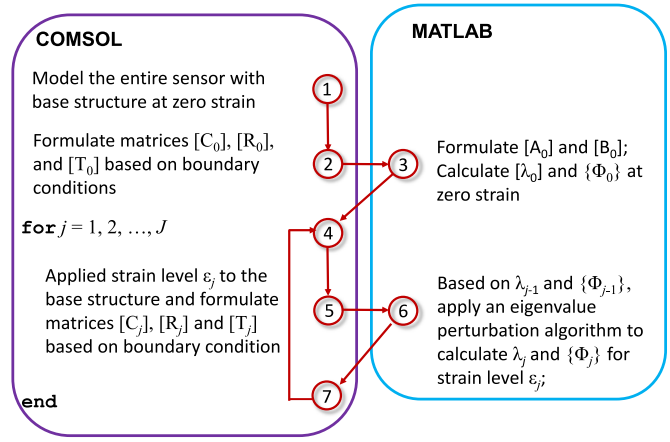

Fig. 8. COMSOL-MATLAB communication.

C. COMSOL-MATLAB Framework

The antenna sensor models can be easily built in COMSOL through user friendly graphical interface, but it is not convenient to implement customized eigenvalue solvers into COMSOL graphical interface. Instead, COMSOL LiveLink for MATLAB allows the customized solvers to be applied to COMSOL-generalized matrices in electromagnetic domain.

Fig. 8 shows the COMSOL-MATLAB communication process using eigenvalue techniques for updating sensor resonance frequencies at multiple strain levels. The simulation model is first built in COMSOL with proper mechanical and electromagnetic boundary conditions. Matrices $[\mathrm{C}_0]$, $[\mathrm{R}_0]$, and $[\mathrm{T}_0]$ in (6) are then generated by COMSOL and transferred to MATLAB. These matrices are used to construct $[\mathrm{A}_0]$ and $[\mathrm{B}_0]$ according to (11). The eigenvalue λ_0 and eigenvector $\{\Phi_0\}$ are calculated through eigenvalue solver at zero strain level ε_0.

Upon the simulation at zero strain level and later at a *j*th strain level, the antenna structure is subjected to corresponding loading in COMSOL. The deformed antenna shape is used to generate inductance and capacitance matrices at strain level ε_j. The corresponding system matrices $[\mathrm{A}_j]$ and $[\mathrm{B}_j]$ are constructed in MATLAB. An eigenvalue perturbation algorithm can then be applied to calculate the eigenvalue λ_j and eigenvector $\{\Phi_j\}$ at strain ε_j, based on λ_{j-1} and $\{\Phi_{j-1}\}$ from the previous strain step. The updating process continues for all required strain levels.

V. Validation Example

To validate the accuracy and efficiency of the proposed partially air-filled cavity model and the IPIRQ eigenvalue

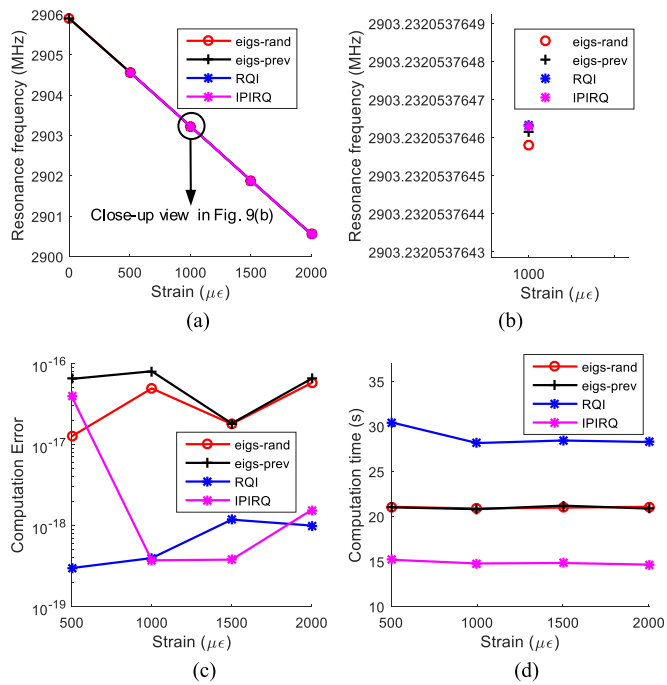

Fig. 9. Eigenfrequency results comparison between `eigs` solvers and proposed method. (a) Eigenfrequencies (Resonance frequencies). (b) Eigenfrequencies (Closed-up view at 1000 $\mu\varepsilon$). (c) Computation error. (d) Computation time.

perturbation algorithm, the same 2.9 GHz patch antenna is investigated. Four strain levels are simulated, ranging 500∼2000 $\mu\varepsilon$ with a strain step of 500 $\mu\varepsilon$. The eigenfrequency at each strain level is first calculated by `eigs` function in MATLAB. To check the effect of different starting vectors to the computation error and time, a randomly generated vector and the eigenvector from previous strain level are adopted as the starting vector, respectively, for comparison. The RQI and the IPIRQ methods are applied for comparison with the two MATLAB eigs solutions with different starting vectors. The error tolerance for the four methods (two eigs, RQI, and IPIRQ) is set to 10^{-16}.

The computed resonance frequency results from the four solvers are compared and summarized in Fig. 9. The legend "eigs-rand" denotes the results from eigs function with randomly generated vector as starting vector; the legend "eigs-prev" indicates results from eigs function with previous eigenvector as starting vector; the legend "RQI" and "IPIRQ" denote the results from the RQI and the IPIRQ methods, respectively. In this example, the resonance frequencies from four solution methods show good match [see Fig. 9(a)] at all strain steps. Fig. 9(b) shows the closed-up view at 1000 $\mu\varepsilon$.

To further compare the solution accuracy, the following error index is defined:

$$\text{error} = \frac{||\mathrm{A}_{j+1}\{\Phi_{j+1}\} - \lambda_{j+1}\mathrm{B}_{j+1}\{\Phi_{j+1}\}||}{||\mathrm{A}_{j+1}|| + ||\lambda_{j+1}\mathrm{B}_{j+1}||} \quad (13)$$

where λ_{j+1} and $\{\Phi_{j+1}\}$ are the computed eigenvalue and eigenvector at $(j+1)$th strain step.

TABLE II
COMPUTATION TIME (SECONDS) OF RQI AND IPIRQ AT 1000 $\mu\varepsilon$

Step	RQI		IPIRQ		
①	0.1802		0.1923		
②	0.0012		0.0014		
③	0.3923		0.4170		
	First iteration	Second iteration			
④	13.4173	13.6476	13.4474		
			First iteration	Second iteration	Third iteration
⑤	0.2135	0.2072	0.2020	0.1855	0.1974
⑥	0.0127	0.0113	0.0124	0.0102	0.0101
⑦	0.0338	0.0384	0.0399	0.0372	0.0334

As shown in Fig. 9(c), the computational errors of all methods are lower than 1×10^{-16}. Computation error for the RQI and the IPIRQ methods is between 3.8×10^{-18} and 4.2×10^{-18}, both smaller than the `eigs` solutions. Comparison of computation time is plotted in Fig. 9(d). The computation time of IPIRQ is the fastest, which is about 1.3 times faster than the `eigs` solutions and 1.86 times faster than the RQI method. To explain the difference between RQI and IPIRQ, Table II provides computation time for every step of these two methods at 1000 $\mu\varepsilon$ level. The step numbers follow Fig. 7. As shown in the table, a critical time-consuming step of both algorithms is LU factorization (Step ④ in both methods). Therefore, although RQI has only two iterations and IPIRQ needs three iterations to converge, IPIRQ is more efficient than RQI by reusing LU factorization while achieving similar accuracy.

VI. SUMMARY AND DISCUSSION

This study first presents electromagnetic finite element formulation of antenna sensors using both frequency domain solver and eigenfrequency solver. The 2.9 GHz patch antenna simulation is performed using both solvers, and the calculated resonance frequency results are compared. The eigenfrequency solver consumes nearly 5% of the time required by the frequency-domain solver, while providing the similar accuracy.

In order to reduce computational loads, two FEM models (cavity and partially air-filled cavity models) are proposed. While the cavity model significantly reduces simulation time, the accuracy is not reliable due to the absence of air volume. It is discovered that the partially air-filled cavity model not only reduces computational efforts but also maintains accuracy for the electromagnetic simulation. To further improve the solution efficiency, two eigenvalue perturbation methods, RQI and IPIRQ are studied. The solution accuracy and efficiency are compared with MATLAB `eigs` command. The results show that the commonly used RQI method achieves high computation accuracy, but it is relatively slower than other solutions. Meanwhile, the proposed IPIRQ method achieves the best balance between accuracy and timing.

Overall, the proposed antenna simulation approach, using partially air-filled model and the IPIRQ eigenvalue perturbation method, provides an eigenvalue solution in 14.82 s for the 2.9 GHz antenna at 1000 $\mu\varepsilon$. In comparison, the conventional frequency domain solver requires 9722 s (2 h, 42 min, 2 s). The efficiency improvement is significant. The proposed approach provides a simulation framework enabling much more efficient antenna sensor designs.

Acknowledgment

Any opinions, findings, and conclusions or recommendations expressed in this publication are those of the authors and do not necessarily reflect the view of the sponsor.

References

[1] E. G. Straser and A. S. Kiremidjian, "A modular, wireless damage monitoring system for structures," John A. Blume Earthquake Eng. Center, Stanford Univ., Stanford, CA USA, Rep. 128, 1998.

[2] J. P. Lynch *et al.*, "Design and performance validation of a wireless sensing unit for structural health monitoring applications," *Struct. Eng. Mech.*, vol. 17, no. 3/4, pp. 393–408, 2004.

[3] Y. Wang, J. P. Lynch, and K. H. Law, "A wireless structural health monitoring system with multithreaded sensing devices: design and validation," *Struct. Infrastruct. Eng.*, vol. 3, no. 2, pp. 103–120, 2007.

[4] J. P. Lynch and K. J. Loh, "A summary review of wireless sensors and sensor networks for structural health monitoring," *The Shock Vib. Dig.*, vol. 38, no. 2, pp. 91–128, 2006.

[5] A. Deivasigamani, A. Daliri, C. H. Wang, and S. John, "A review of passive wireless sensors for structural health monitoring," *Mod. Appl. Sci.*, vol. 7, no. 2, pp. 57–76, 2013.

[6] J. C. Butler, A. J. Vigliotti, F. W. Verdi, and S. M. Walsh, "Wireless, passive, resonant-circuit, inductively coupled, inductive strain sensor," *Sensors Actuators A, Phys.*, vol. 102, no. 1/2, pp. 61–66, 2002.

[7] K. J. Loh, J. P. Lynch, and N. A. Kotov, "Inductively coupled nanocomposite wireless strain and pH sensors," *Smart Struct. Syst.*, vol. 4, no. 5, pp. 531–548, 2008.

[8] Y. Jia, K. Sun, F. J. Agosto, and M. T. Quinones, "Design and characterization of a passive wireless strain sensor," *Meas. Sci. Technol.*, vol. 17, no. 11, pp. 2869–2876, 2006.

[9] A. Daliri, A. Galehdar, S. John, C. H. Wang, W. S. T. Towe, and K. Ghorbani, "Wireless strain measurement using circular microstrip patch antennas," *Sensors Actuators A, Phys.*, vol. 184, no. 1, pp. 86–92, 2012.

[10] S. Deshmukh and H. Huang, "Wireless interrogation of passive antenna sensors," *Meas. Sci. Technol.*, vol. 21, no. 3, 2010, Art. no. 035201, 9 pp.

[11] X. Xu and H. Huang, "Battery-less wireless interrogation of microstrip patch antenna for strain sensing," *Smart Mater. Struct.*, vol. 21, no. 12, 2012, Art. no. 125007.

[12] X. Yi, C. Cho, J. Cooper, Y. Wang, M. M. Tentzeris, and R. T. Leon, "Passive wireless antenna sensor for strain and crack sensing-electromagnetic modeling, simulation, and testing," *Smart Mater. Struct.*, vol. 22, no. 8, 2013, Art. no. 085009.

[13] X. Yi, T. Wu, Y. Wang, R. T. Leon, M. M. Tentzeris, and G. Lantz, "Passive wireless smart-skin sensor using RFID-based folded patch antennas," *Int. J. Smart Nano Mater.*, vol. 2, no. 1, pp. 22–38, 2011.

[14] C. Cho, X. Yi, D. Li, Y. Wang, and M. M. Tentzeris, "Passive wireless frequency doubling antenna sensor for strain and crack sensing," *IEEE Sensors J.*, vol. 16, no. 14, pp. 5725–5733, 2016.

[15] C. Cho, X. Yi, D. Li, Y. Wang, and M. M. Tentzeris, "Passive wireless frequency doubling antenna sensor for strain and crack sensing," *IEEE Sensors J.*, vol. 16, no. 14, pp. 5725–5733, Jul. 2016.

[16] X. Yi, Y. Wang, M. M. Tentzeris, and R. T. Leon, "Multi-physics modeling and simulation of a slotted patch antenna for wireless strain sensing " in *Proc. 9th Int. Workshop Struct. Health Monit.*, Stanford, CA, USA, 2013, pp. 1857–1864.

[17] K. R. Carver and J. M. Mink, "Microstrip antenna technology," *IEEE Trans. Antennas Propag.*, vol. AP-27, no. 1, pp. 2–24, Jan. 1981.

[18] P. Daly, "Hybrid-mode analysis of microstrop by finite-element methods," *IEEE Trans. Microw. Theory Techn.*, vol. MTT-19, no. 1, pp. 19–25, Jan. 1971.

[19] B. N. Parlett, "The Rayleigh quotient iteration and some generalizations for nonnormal matrices," *Math. Comput.*, vol. 28, no. 127, pp. 679–693, 1974.

[20] A. Amiraslani and P. Lancaster, "Rayleigh quotient algorithms for nonsymmetric matrix pencils," *Numer. Algorithms*, vol. 51, pp. 5–22, 2009.

[21] J. H. Wilkinson, *The Algebraic Eigenvalue Problem*. Oxford, U.K.: Clarendon, 1965.

[22] J. M. Jin, *The Finite Element Method in Electromagnetics*. 2nd ed. New York, NY, USA: Wiley, 2002.

[23] W. C. Chew and W. H. Weedon, "A 3-D perfectly matched medium from modified Maxwell's equations with stretched coordinates," *Microw. Opt. Technol. Lett.*, vol. 7, no. 13, pp. 599–604, 1994.

[24] J. L. Volakis, A. Chatterjee, and L. C. Kempel, "*Finite Element Method for Electromagnetics: Antenna, Microwave Circuits, and Scattering*," New York, NY, USA: IEEE Press, 1998.

[25] H. Guo, B. Oswald, and P. Arbenz, "3-dimensional eigenmodal analysis of plasmonic nanostructures," *Opt. Exp.*, vol. 20, no. 5, pp. 5481–5500, 2012.

[26] A. Chatterjee, J. M. Jin, and J. L. volakis, "Edge-based finite elements and vector ABC's applied to 3-D scattering," *IEEE Trans. Antennas Propag.*, vol. 41, no. 2, pp. 221–226, Feb. 1993.

[27] F. Tisseur and K. Meerbergen, "The quadratic eigenvalue problem," *SIAM Rev.*, vol. 43, no. 2, pp. 235–286, 2001.

[28] T. G. Wright and L. N. Trefethen, "Large-scale computation of pseudospectra using ARPACK and eigs," *J. Sci. Comput.*, vol. 23, no. 2, pp. 591–605, 2001.

[29] J. A. George and J. W.-H. Liu, C*omputer Solution of Large Sparse Positive Definite Systems*. Hanford, CA, USA: Prentice-Hall, 1981.

Chunhee Cho Cho received the M.S degree in electrical and computer engineering and Ph.D. degree in civil and environmental engineering from the Georgia Institute of Technology, Atlanta, GA, USA, both in 2016.

He was with the Republic of Korea Marine Corps as an Engineering Officer (First Lieutenant) from 2003 to 2006. He was with Hyundai Architects & Engineering Associates, as a Structure Engineer from 2009 to 2010. His research interests include structural health monitoring, passive wireless strain sensing, and sensor design optimization.

Xiaohua Yi received the M.S. degree in electrical and computer engineering from the Georgia Institute of Technology, Atlanta, GA, USA, and Ph.D. degree from the School of Civil and Environmental Engineering, Georgia Institute of Technology, in 2013 and 2014, respectively.

He has been working in the field of multiphysics modeling, embedded algorithm design, wireless antenna sensors design, and signal processing to develop robust inspection systems that can be used for field applications. He is currently a Senior Research Engineer with the ExxonMobil Upstream Research Company, Houston, TX, USA. His general interests include remote sensing technology, smart material and structural systems development, and multiphysics modeling. His research has resulted in the publication of more than 30 journal and conference papers.

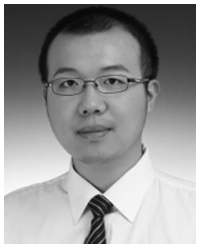

Dan Li received the B.S. and M.S. degrees from the School of Civil Engineering, Tongji University, Shanghai, China, in 2011 and 2014, respectively. He is currently working toward the Ph.D. degree in civil engineering at the School of Civil and Environmental Engineering, Georgia Institute of Technology, Atlanta, GA, USA.

His primary research interests include passive sensing technology, multiphysics simulation, and structural health monitoring.

Yang Wang (S'06–M'07) received the B.S. and M.S. degrees in civil engineering from Tsinghua University, Beijing, China, and the M.S. degree in electrical engineering and Ph.D. degree in civil engineering from Stanford University, Stanford, CA, USA.

He is an Associate Professor with the School of Civil and Environmental Engineering, Georgia Institute of Technology, Atlanta, GA, USA. His research interests include structural health monitoring and damage detection, decentralized structural control, wireless and mobile sensors, and structural dynamics.

Dr. Wang has served as an Associate Editor for the ASCE's (American Society of Civil Engineers) *Journal of Bridge Engineering* since 2011. He was the recipient of an NSF Early Faculty Career Development (CAREER) Award in 2012 and a Young Investigator Award from the Air Force Office of Scientific Research (AFOSR) in 2013.

Manos M. Tentzeris (S'94–M'98–SM'03–F'10) is a Professor with the School of Electrical and Computer Engineering, Georgia Institute of Technology, Atlanta, GA, USA. He is the Associate Editor of the IEEE TRANSACTIONS ON MICROWAVE THEORY AND TECHNIQUES, the IEEE TRANSACTIONS ON ADVANCED PACKAGING, and the *International Journal on Antennas and Propagation*.

Prof. Tentzeris is the founder and the Chair of the RFID Technical Committee of the IEEE MTT Society and the Secretary/Treasurer of the IEEE C-RFID. He is a member of URSI-Commission D, a member of the MTT-15 Committee, an Associate Member of EuMA, a Fellow of the Electromagnetic Academy, and a member of the Technical Chamber of Greece. He was the recipient/co-recipient of numerous awards including the 2015 IET Microwaves, Antennas and Propagation Premium Award, the 2013 IET Microwaves, Antennas and Propagation Premium Award, the 2010 IEEE Antennas and Propagation Society Piergiorgio L. E. Uslenghi Letters Prize Paper Award, the 2006 IEEE MTT Outstanding Young Engineer Award, and the 2000 NSF CAREER Award.